



Thermal state of the upper mantle beneath the Northern Cordilleran Volcanic Province (NCVP), British Columbia, Canada

M. Harder, J.K. Russell*

Volcanology and Petrology Laboratory, Earth and Ocean Sciences, The University of British Columbia, Vancouver, B.C., Canada V6T 1Z4

Received 30 July 2004; accepted 25 May 2005
Available online 2 August 2005

Abstract

Data are presented for a suite of peridotitic mantle-derived xenoliths collected from basanite lavas within the Llangorse volcanic field, northwest British Columbia. The xenoliths comprise spinel lherzolite and subordinate spinel harzburgite. Two-pyroxene thermometry based on the Brey and Köhler (1990) [Brey, G.P., Köhler, T., 1990. Geothermobarometry in four-phase lherzolites II. New thermobarometers, and practical assessment of existing thermobarometers. *Journal of Petrology*, 31, 1353–1378.] calibration was applied to 44 xenolith samples. The resulting geothermometry define minimum (800–850 °C) and maximum (1050–1100 °C) temperatures of equilibration for the xenolith suite which are estimates of thermal conditions in the underlying lithospheric mantle. We take the minimum temperatures as indicative of the maximum MOHO temperature; the maximum xenolith temperatures provide a minimum temperature for the transition from lithospheric to asthenospheric mantle. The geothermometry data are combined with published heat flow data to produce a set of model geotherms for this portion of the northern Cordillera. The model geotherms constrain the thickness of the mantle lithosphere in the northern Canadian Cordillera to between 16 and 30 km, corresponding to depths to the lithosphere/asthenosphere boundary of 52–66 km. We show that this model is consistent with an underlying convecting asthenospheric mantle with an average temperature and viscosity of 1210–1250 °C and $10^{19.4}$ Pa s, respectively. We conclude by exploring the implications this model has for the source regions of alkaline magmas erupted over this portion of the northern Cordilleran volcanic province.

© 2005 Elsevier B.V. All rights reserved.

Keywords: Mantle lithosphere; Canadian Cordillera; Geothermometry; Peridotite; Xenolith; Northern Cordilleran volcanic province

1. Introduction

The mantle lithosphere underlying the northern Canadian Cordillera has been the focus of geophysical and petrological research aimed at understanding the

physical and chemical character of the Cordilleran lithosphere, the origins of the underlying mantle lithosphere and, ultimately, the mechanisms of crustal amalgamation (Clowes et al., 1999; Hyndman and Lewis, 1999; Hammer et al., 2000; Snyder et al., 2002; Lewis et al., 2003; Hammer and Clowes, 2004). For example, the northern Canadian Cordillera became welded to the western margin of North Amer-

* Corresponding author.

E-mail address: krussell@eos.ubc.ca (J.K. Russell).

ica beginning in the Middle Jurassic (Coney et al., 1980; Monger et al., 1982), yet the nature and origin of the lithospheric mantle underlying these amalgamated crustal terranes remains a major uncertainty.

The Canadian Cordillera is ideal for direct study of the mantle lithosphere because of the presence of Miocene to Holocene mafic alkaline volcanic rocks

(Fig. 1; Edwards and Russell, 1999, 2000). Lavas from these volcanic centres commonly contain peridotite xenoliths, providing primary samples of the mantle lithosphere underlying the northern Cordillera. Numerous previous workers have taken advantage of these occurrences of mantle xenoliths within Miocene to Holocene volcanic rocks distributed across the

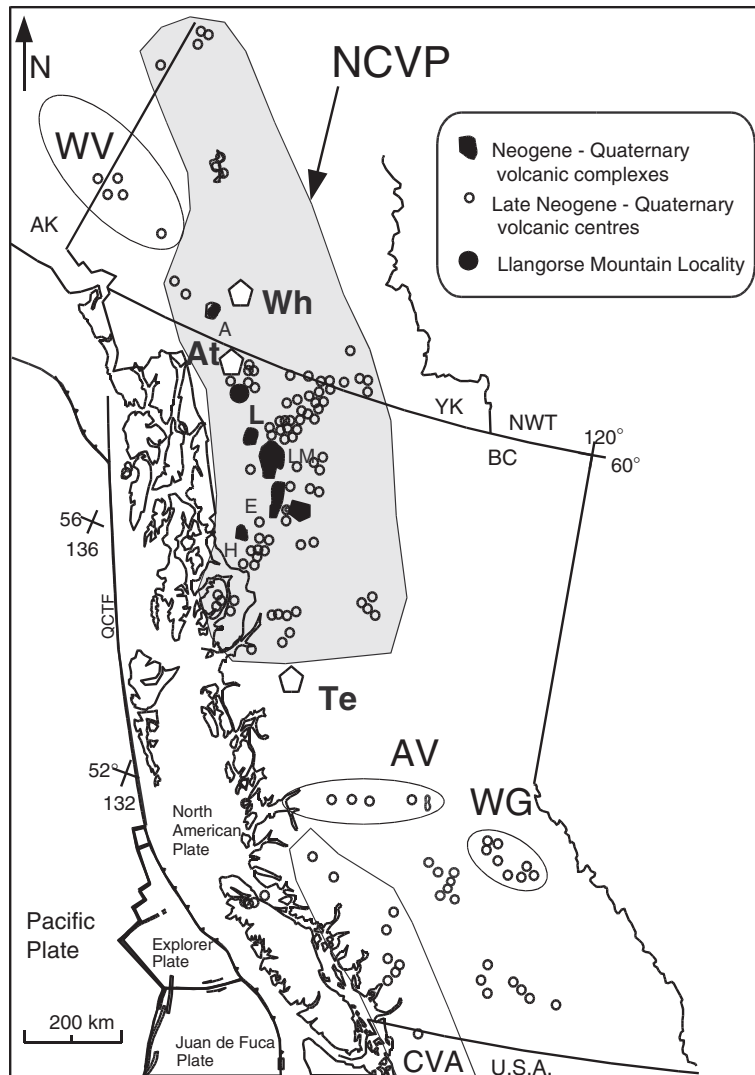


Fig. 1. The northern Cordilleran volcanic province (NCVP) comprises Miocene and younger volcanic rocks distributed across northern British Columbia (BC), the Yukon territory (YK) and easternmost Alaska (AK) (Edwards and Russell, 2000). Other major volcanic provinces include: Wrangell volcanics (WV), Anaheim volcanic belt (AV), Wells–Grey volcanic field (WG), and Cascade volcanic arc (CVA). Major centres include Hoodoo Mountain (H), Mount Edziza (E), Alligator Lake (A), and Level Mountain (LM). Small black circles represent individual occurrences of Miocene to Holocene volcanic rocks. This study involves volcanic rocks from near Llangorse Mountain (L) immediately southeast of Atlin (At). Other population centers include Whitehorse (Wh) and Terrace (Te). The Queen Charlotte transform fault (QCTF) defines the boundary between the Pacific and North American plates.

Canadian Cordillera (i.e., Littlejohn and Greenwood, 1974; Ross, 1983; Brearley and Scarfe, 1984; Brearley et al., 1984; Canil et al., 1987; Shi et al., 1998; Peslier et al., 2000a,b).

The purpose of our study is to explore the utility of mineralogical and chemical information within peridotite xenoliths for constraining the thermal state of the crustal and mantle lithosphere. Here, we present field observations, petrographic descriptions, and chemical data on a large suite of peridotite xenoliths collected from Llangorse Mountain. We use two-pyroxene thermometry on peridotite xenoliths (Brey and Köhler, 1990) to recover as wide a range of temperatures as possible from the lithospheric mantle. These data constrain the temperatures at the base of the crust (MOHO) and at the base of the mantle lithosphere and are used, in conjunction with heat flow data, to infer the temperature and thickness of the lithospheric mantle underlying the northern Cordillera.

2. Location and previous work

The northern Cordilleran volcanic province (NCVP; Fig. 1), as defined by Edwards and Russell (1999, 2000), is one of the largest Miocene to Holocene volcanic provinces in western North America and comprises dominantly mafic, Miocene to Holocene alkaline volcanic rocks. The volcanism is proposed to result from extensional forces acting on the northern Cordilleran lithosphere (Edwards and Russell, 1999, 2000). The NCVP is mainly expressed as small volume, short-lived basaltic volcanoes or erosional remnants of centres (Fig. 1), in contrast to several longer-lived edifices (e.g., Mt. Edziza, Level Mtn., Hoodoo Mtn.; Fig. 1). The volcanism is distributed across northwestern British Columbia, the Yukon Territory, and eastern Alaska (Edwards and Russell, 2000), and is bounded by the Tintina fault system to the east and the Denali-Coast fault system to the west.

The Llangorse volcanic field (LVF; Edwards et al., 2003; Harder et al., 2003) covers approximately 144 km² and is centred on Llangorse Mountain, approximately 55 km southeast of Atlin, BC (Fig. 1). The LVF lies entirely within the Intermontane belt and is underlain mainly by the Llangorse Mountain pluton and by minor amounts of Cache Creek Group cherts (Aitken, 1959). There are seven volcanic localities

within the LVF, consisting of eroded remnants of lava flows and exposed feeder dykes (Table 1).

Volcanic rocks in the LVF have been studied by numerous groups, including as part of broad-scale geochemical studies across the northern Cordillera (Carignan et al., 1994; Abraham et al., 2001) and detailed petrological studies of specific volcanic centres (e.g., Hirschfeld Creek; Higgins and Allen, 1985; Francis and Ludden, 1995). The peridotitic xenoliths found in several of the LVF volcanic localities have also been the focus of study. Detailed petrology (e.g., petrography, chemistry and thermometry) of peridotite xenoliths have been used to address the physical and chemical composition (Nicholls et al., 1982; Brearley and Scarfe, 1984; Brearley et al., 1984; Canil et al., 1987; Nicholls and Stout, 1996, 1997; Shi et al., 1998; Peslier et al., 2000b), the age and origin (Nicholls et al., 1982; Brearley and Scarfe, 1984; Peslier et al., 2000a), and the thermal state of the underlying mantle (Nicholls et al., 1982; Brearley et al., 1984; Canil et al., 1987; Shi et al., 1998).

Table 1

Major element chemical compositions of lava samples (MH-02-) from the LVF including replicate (split and duplicate) analyses of some samples

Sample	101	101r	101s	101s	112	160	173	213
Center	LM	LM	LM	LM	LM	LP	TH	HR
SiO ₂	45.13	44.99	44.91	45.00	44.11	41.47	40.57	45.57
TiO ₂	2.23	2.21	2.20	2.22	1.92	2.72	2.53	2.05
Al ₂ O ₃	13.12	13.13	13.15	13.18	12.36	11.99	11.70	13.37
Fe ₂ O ₃	2.23	2.59	2.80	2.73	2.63	5.37	6.70	2.76
FeO	10.09	9.68	9.59	9.59	9.76	8.35	7.57	9.58
MnO	0.18	0.18	0.18	0.18	0.18	0.19	0.21	0.19
MgO	11.69	11.61	11.65	11.68	13.55	12.02	10.67	11.04
CaO	9.96	9.96	9.94	9.99	10.24	9.18	9.45	9.37
Na ₂ O	3.14	3.12	3.11	3.15	2.34	4.52	5.22	2.81
K ₂ O	1.23	1.22	1.22	1.22	1.07	1.79	1.76	1.01
P ₂ O ₅	0.50	0.50	0.50	0.51	0.43	1.00	1.30	0.38
Total	99.51	99.19	99.25	99.45	98.59	98.61	97.68	98.13
Rock type ^a :	Bas	Bas	Bas	Bas	Bas	Neph	Neph	AOB
<i>Thermodynamic liquidus (1 atm., anhydrous) properties^b</i>								
T(°C)	1301	1296	1296	1297	1331	1305	1263	1285
X _{Fo}	86.9	87.2	87.4	87.4	88.5	90	90	86.7

The localities are Llangorse Mountain (LM), Lone Point (LP), Table Hill (TH), and Hidden Ridge (HR).

^a Rock types: basanite (Bas), olivine nephelinite (Neph), alkali-olivine basalt (AOB), based on an Alkali-Silica plot.

^b T(°C) and olivine saturation composition (X_{Fo}) calculated using MELTS (Ghiorso and Sack, 1995).

Table 2

Whole rock chemical analyses (wt.%) of samples of peridotite xenoliths collected from basanite lavas at Llangorse Mountain

Label	19	100	104	108	110	111	113	114	115	117	118	120	121 (N=4)	122	123 (N=4)	125	112	19b	95LM-1 (N=6)
SiO ₂	43.55	43.98	43.87	43.80	44.42	44.14	43.20	42.97	43.73	44.05	43.56	43.41	43.97	43.75	43.84	43.76	43.76	43.81	43.56
TiO ₂	0.075	0.024	0.040	0.050	0.070	0.152	0.039	0.028	0.032	0.024	0.014	0.025	0.035	0.018	0.021	0.047	0.016	0.020	0.013
Al ₂ O ₃	1.00	0.88	1.83	1.77	3.31	3.37	0.74	0.65	0.87	0.90	0.63	0.69	2.34	1.80	1.68	2.59	0.79	0.85	0.68
Fe ₂ O ₃	1.47	1.45	1.53	1.74	1.99	1.76	1.69	1.32	1.40	1.81	1.57	2.02	1.88	1.49	1.60	1.62	1.75	1.79	1.65
FeO	6.37	6.10	6.04	6.47	6.13	7.13	6.02	6.35	6.21	6.11	6.10	5.89	6.27	6.58	6.42	6.97	5.82	6.14	5.87
MnO	0.12	0.11	0.12	0.12	0.12	0.13	0.12	0.11	0.12	0.12	0.12	0.12	0.12	0.12	0.12	0.13	0.112	0.120	0.11
MgO	45.49	45.94	43.47	43.39	39.43	38.91	46.57	46.82	45.93	45.17	46.81	45.92	42.09	42.98	43.64	40.90	45.85	45.50	46.46
CaO	0.83	0.66	1.59	1.49	3.25	3.25	0.61	0.58	0.70	0.75	0.53	0.65	2.27	1.81	1.64	2.73	0.60	0.73	0.52
Na ₂ O	0.10	0.00	0.24	0.10	0.28	0.24	0.13	0.04	0.08	0.05	0.03	0.01	0.09	0.04	0.04	0.10	0.32	0.27	0.30
K ₂ O	0.09	0.02	0.17	0.01	0.01	0.03	0.09	0.05	0.05	0.02	0.01	0.04	0.01	0.01	0.02	0.01	0.02	0.02	0.01
P ₂ O ₅	0.027	0.014	0.055	0.011	0.011	0.013	0.018	0.016	0.015	0.014	0.009	0.032	0.010	0.009	0.009	0.011	0.020	0.012	0.010
Total	99.12	99.18	98.95	98.95	99.02	99.12	99.22	98.94	99.14	99.01	99.37	98.81	99.08	98.60	99.01	98.87	99.07	99.26	99.18
Fe ₂ O ₃ (T)	8.55	8.23	8.24	8.93	8.80	9.68	8.38	8.38	8.30	8.60	8.35	8.57	8.84	8.80	8.73	9.37	8.23	8.62	8.18
LOI	0.37	0.03	0.29	0.12	0.13	0.26	0.09	0.16	0.07	0.30	−0.03	0.09	0.03	0.15	0.15	0.17	<d/l	<d/l	0.00
Mg#	0.88	0.88	0.88	0.87	0.87	0.85	0.89	0.88	0.88	0.88	0.88	0.89	0.87	0.87	0.87	0.85	0.89	0.88	0.89
Fe ₂ O ₃ /FeO	0.23	0.24	0.25	0.27	0.32	0.25	0.28	0.21	0.23	0.30	0.26	0.34	0.30	0.23	0.25	0.23	0.30	0.29	0.28
<i>Trace element content (ppm)</i>																			
Cr	4413	4650	4042	4129	4503	3810	3881	3889	4347	4294	3970	5581	4339	4141	4186	4084	4685	4448	4662
Ni	2471	2517	2332	2429	2169	2063	2576	2632	2545	2482	2584	2527	2377	2396	2449	2312	2513	2509	2528
Sc	6	6	13	8	16	17	8	8	6	4	8	6	14	15	8	13	11	<d/l	7
V	32	22	32	47	70	82	23	17	20	28	18	26	58	50	44	58	29	32	19

Sample labels have prefix MH-02 except for LM samples. Averages are reported for multiple (N) replicate analyses.

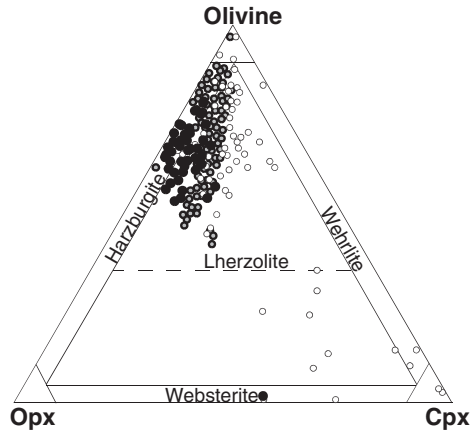


Fig. 2. Modal mineralogy of peridotite samples from Llangorse Mountain (black circles) and other localities in the NCVP (gray circles; Shi et al., 1998) or from central and southern British Columbia (open circles; Littlejohn and Greenwood, 1974). Modes for Llangorse samples are from Rietveld X-ray diffraction analysis (Rietveld, 1967; Raudsepp et al., 1999), bulk chemical analyses (e.g., computed), or from visual estimations on hand-samples and thin sections.

This study focuses on mantle-derived xenoliths collected from lavas exposed near Llangorse Mountain. The lava is interpreted to represent an erosional remnant of a

valley-filling lava flow overlying syngenetic debris flow sediments (see Harder and Russell, in review'04). These lavas are basanitic in composition (Nos. 101 and 112; Table 1) having 5–8 wt.% normative nepheline and contain abundant fresh peridotite xenoliths.

3. Petrography of peridotites

A suite of more than 80 peridotite xenoliths was collected from the basanite lava flow and the underlying volcanoclastic sediments at Llangorse Mountain (Table 2). Most xenolith samples are <5 cm in size, but many exceed 10 cm in diameter and the largest are approximately 25 cm in diameter. All peridotites are spinel-bearing; we observed no garnet or spinel–garnet peridotite xenoliths. Approximately 60% of the xenolith samples are harzburgite and 40% are lherzolite (Fig. 2; Table 4). A single sample was collected in which the host peridotite was cut by a vein of spinel websterite (pyroxenite).

With the exception of the websterite sample, most xenoliths are coarse grained and equigranular. Coarse-grained peridotite samples usually have equilibrium

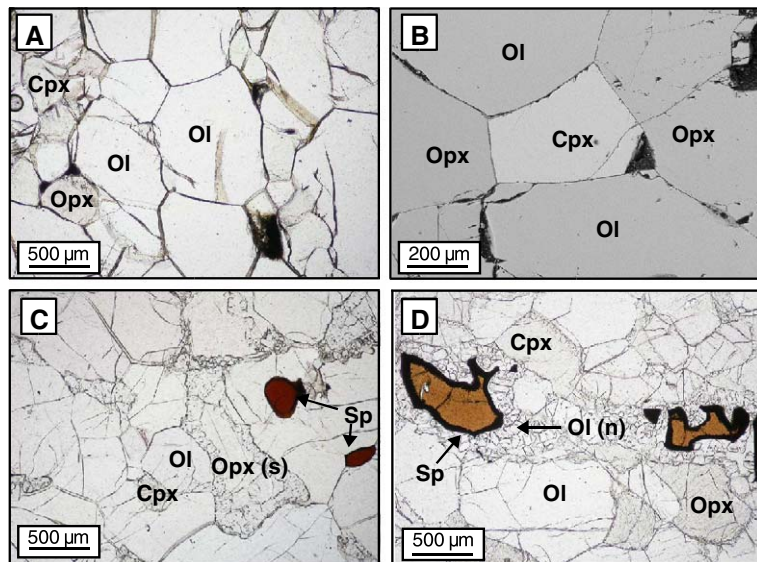


Fig. 3. Photomicrographs and SEM images of peridotite samples. (A) Microscope and (B) SEM images of coarse grained peridotite dominated by triple-point grain boundaries between olivine (Ol), orthopyroxene (Opx), and clinopyroxene (Cpx) suggesting attainment of textural equilibrium. (C) Photomicrograph image of coarse grained spinel (Sp) peridotite showing sieve-textured coronas of orthopyroxene (Opx(s)) suggesting a relatively late thermal disturbance; cores of orthopyroxene are generally unmodified. (D) Photomicrograph showing break-down of spinel (Sp) in some samples; relict grains of spinel are surrounded by neoblasts of olivine (Ol(n)).

Table 3

Representative chemical compositions (wt.%) of orthopyroxene (Opx) and clinopyroxene (Cpx) mineral pairs from each sample (MH-02-)

Opx	110	108	111	10	9c	9b	10b	109b	18b	104	100	115	122	117	5b	8b	4A	9d	10c	10d
SiO ₂	54.42	55.64	55.08	54.90	56.94	56.55	55.36	54.85	56.51	55.33	56.92	56.56	55.15	55.50	56.28	56.01	54.78	56.22	56.03	54.47
TiO ₂	0.08	0.09	0.14	0.12	0.02	0.00	0.01	0.00	0.05	0.01	0.02	0.00	0.07	0.04	0.00	0.00	0.01	0.07	0.00	0.07
Al ₂ O ₃	3.99	3.43	4.27	4.61	2.03	1.70	3.27	2.49	1.50	3.52	2.12	1.90	3.81	2.36	1.83	2.29	2.89	0.80	2.49	4.67
Cr ₂ O ₃	0.34	0.38	0.27	0.44	0.58	0.46	0.39	0.64	0.74	0.46	0.55	0.44	0.38	0.59	0.47	0.43	0.50	0.44	0.47	0.43
FeO	6.26	5.89	6.99	6.19	5.28	5.12	5.67	5.49	5.28	5.58	5.28	5.23	6.64	5.53	5.27	5.66	5.73	5.38	5.14	5.93
MnO	0.19	0.17	0.14	0.16	0.13	0.10	0.14	0.10	0.13	0.16	0.08	0.15	0.18	0.13	0.12	0.13	0.12	0.17	0.13	0.12
MgO	33.41	33.94	32.98	32.85	34.89	34.62	34.07	34.06	34.29	34.01	35.22	35.06	33.62	34.82	35.46	34.93	34.61	34.87	34.80	33.71
NiO	0.06	0.10	0.08	0.05	0.10	0.08	0.01	0.07	0.10	0.05	0.07	0.09	0.13	0.07	0.07	0.07	0.08	0.08	0.10	0.05
CaO	0.50	0.49	0.49	0.98	0.67	0.69	0.55	0.67	1.31	0.51	0.71	0.73	0.51	0.76	0.66	0.53	0.51	1.62	0.72	0.51
Na ₂ O	0.03	0.06	0.07	0.10	0.05	0.01	0.03	0.04	0.05	0.02	0.00	0.01	0.04	0.04	0.03	0.00	0.00	0.07	0.05	0.04
Total	99.28	100.19	100.52	100.40	100.70	99.33	99.51	98.41	99.96	99.66	100.97	100.18	100.51	99.83	100.20	100.06	99.22	99.71	99.94	100.01
Cpx	110	108	111	10	9c	9b	10b	109b	18b	104	100	115	122	117	5b	8b	4A	9d	10c	10d
SiO ₂	51.85	52.06	51.55	51.95	53.55	53.73	52.57	53.18	53.86	52.09	53.29	53.22	51.38	52.91	53.82	53.25	51.94	51.57	52.37	52.09
TiO ₂	0.27	0.31	0.79	0.45	0.12	0.02	0.03	0.03	0.00	0.06	0.03	0.00	0.23	0.01	0.00	0.04	0.02	0.11	0.00	0.16
Al ₂ O ₃	6.20	5.58	6.63	6.67	3.08	1.47	3.52	2.44	2.46	5.06	1.94	1.93	4.87	2.53	1.73	2.45	3.17	4.76	2.58	5.52
Cr ₂ O ₃	0.79	0.15	0.67	0.91	1.47	0.67	0.86	0.81	0.83	1.15	0.69	0.69	0.69	0.81	0.70	0.82	0.97	0.72	0.75	0.76
FeO	2.47	2.45	2.88	2.58	1.96	1.86	1.95	1.94	2.21	2.17	1.97	1.88	2.47	2.27	1.91	2.14	2.33	2.20	2.28	2.28
MnO	0.05	0.08	0.09	0.10	0.08	0.07	0.11	0.05	0.06	0.10	0.09	0.08	0.08	0.15	0.08	0.09	0.09	0.10	0.06	0.06
MgO	15.16	15.23	14.99	14.72	16.72	18.20	16.59	17.36	17.58	15.98	18.35	18.16	16.08	17.73	18.37	17.64	17.12	16.29	17.74	16.12
NiO	0.03	0.00	0.04	0.06	0.02	0.00	0.08	0.05	0.00	0.07	0.08	0.08	0.03	0.04	0.05	0.04	0.00	0.02	0.05	0.03
CaO	20.78	20.78	20.94	20.73	21.19	23.30	22.81	23.21	21.24	22.07	23.18	23.15	21.96	21.78	23.21	23.19	22.89	22.04	21.92	21.92
Na ₂ O	1.56	1.54	1.40	1.81	1.23	0.15	0.78	0.34	1.02	1.03	0.15	0.15	0.92	0.87	0.19	0.31	0.53	0.85	0.75	0.94
Total	99.17	98.18	99.97	99.98	99.42	99.49	99.30	99.40	99.27	99.78	99.77	99.35	98.71	99.11	100.08	99.98	99.05	98.66	98.49	99.87
T_{Wells} (°C)	913	894	926	889	953	953	863	915	991	902	969	962	907	956	963	931	896	909	962	938
$T_{\text{B&K}}$ (°C)	926	903	945	900	955	909	809	870	1001	884	936	928	883	956	938	898	859	917	946	931
$ \Delta T $	13	9	18	11	2	44	55	45	10	18	33	34	24	1	25	33	37	9	16	6

Calculated temperatures are reported for each mineral pair using both the Brey and Kohler (1990) and Wells (1977) thermometers.

Table 3 (continued)

Opx	15	12	109	112	124	20	19	102	113	114	115b	116	117b	118	119	120	121	123	125	95LM1	19b
SiO ₂	54.65	56.83	55.68	56.58	53.19	53.95	55.37	55.42	56.63	57.33	55.97	56.73	56.46	56.45	55.90	56.25	54.13	55.35	56.00	56.35	56.29
TiO ₂	0.03	0.05	0.02	0.00	0.09	0.10	0.15	0.06	0.02	0.13	0.00	0.01	0.04	0.00	0.03	0.01	0.02	0.02	0.03	0.00	0.00
Al ₂ O ₃	3.97	0.83	3.05	2.00	6.79	4.08	2.46	3.52	1.87	0.63	2.15	1.90	2.36	1.58	2.41	2.00	3.83	3.68	2.37	1.93	2.30
Cr ₂ O ₃	0.45	0.48	0.72	0.47	0.20	0.56	0.61	0.40	0.51	0.51	0.52	0.51	0.55	0.45	0.53	0.46	0.36	0.46	0.50	0.50	0.51
FeO	6.00	5.84	5.50	5.30	7.82	6.43	5.35	6.05	5.12	5.16	5.37	5.07	5.45	5.33	5.47	5.26	5.77	5.94	5.38	5.29	5.37
MnO	0.16	0.17	0.10	0.15	0.17	0.11	0.13	0.10	0.13	0.11	0.09	0.10	0.13	0.13	0.08	0.17	0.14	0.18	0.08	0.08	0.16
MgO	33.80	34.22	34.39	34.88	31.73	33.94	34.99	34.20	35.11	34.62	34.88	35.56	35.36	35.30	35.22	34.72	33.59	33.63	34.21	35.08	34.86
NiO	0.08	0.11	0.10	0.06	0.07	0.00	0.07	0.09	0.06	0.07	0.07	0.06	0.11	0.06	0.12	0.08	0.13	0.07	0.13	0.11	0.13
CaO	0.55	1.72	0.90	0.62	0.60	0.57	0.72	0.53	0.67	1.69	0.76	0.66	0.68	0.67	0.62	0.65	0.51	0.55	0.72	0.61	0.65
Na ₂ O	0.02	0.07	0.10	0.08	0.09	0.05	0.04	0.04	0.01	0.08	0.02	0.00	0.04	0.00	0.00	0.02	0.03	0.02	0.02	0.03	0.04
Total	99.69	100.31	100.56	100.16	100.75	99.80	99.89	100.42	100.13	100.33	99.83	100.61	101.17	99.97	100.38	99.62	98.50	99.90	99.45	99.98	100.31
Cpx	15	12	109	112	124	20	19	102	113	114	115b	116	117b	118	119	120	121	123	125	95LM1	19b
SiO ₂	52.45	52.02	52.49	53.58	51.22	51.20	51.43	51.74	53.64	53.35	53.47	53.61	53.29	52.93	53.03	52.92	51.41	52.10	52.69	53.77	53.32
TiO ₂	0.14	0.23	0.06	0.00	0.59	0.34	0.25	0.25	0.01	0.00	0.00	0.00	0.04	0.00	0.02	0.02	0.16	0.07	0.02	0.00	0.00
Al ₂ O ₃	4.44	5.21	3.70	3.19	8.91	5.79	2.92	5.30	1.85	1.89	1.94	1.77	2.45	1.57	2.18	1.97	4.84	4.17	2.30	1.68	2.12
Cr ₂ O ₃	0.85	0.98	1.31	1.75	0.26	1.15	1.10	0.95	0.76	0.85	0.70	0.70	0.85	0.68	0.79	0.73	0.86	1.00	0.78	0.61	0.69
FeO	2.15	2.29	2.45	1.91	2.87	2.46	2.17	2.26	2.02	2.08	1.98	1.92	2.24	2.03	2.01	1.92	2.29	2.39	2.03	1.96	2.08
MnO	0.07	0.08	0.11	0.09	0.06	0.07	0.05	0.05	0.06	0.05	0.06	0.06	0.09	0.12	0.07	0.07	0.09	0.03	0.07	0.07	0.02
MgO	16.47	15.98	17.24	16.98	14.26	15.49	17.46	15.87	18.09	18.22	18.26	18.53	17.68	18.59	18.27	17.94	15.92	16.55	17.99	18.24	17.91
NiO	0.13	0.05	0.07	0.05	0.02	0.00	0.04	0.02	0.02	0.04	0.08	0.11	0.02	0.10	0.06	0.04	0.04	0.06	0.08	0.01	0.02
CaO	22.20	21.58	20.36	20.97	20.16	21.14	22.06	21.89	23.43	23.23	23.17	22.92	21.97	23.25	23.26	23.03	22.22	22.96	22.82	23.47	22.88
Na ₂ O	0.82	1.05	1.07	1.22	1.80	1.33	0.56	1.05	0.10	0.10	0.16	0.17	0.77	0.07	0.17	0.21	0.90	0.56	0.17	0.12	0.27
Total	99.73	99.47	98.85	99.73	100.16	98.96	98.04	99.38	99.99	99.80	99.82	99.78	99.40	99.33	99.86	98.86	98.73	99.89	98.95	99.93	99.31
$T_{\text{Wells}} (^{\circ}\text{C})$	930	934	1034	983	934	911	962	906	954	977	968	992	963	965	958	952	881	906	982	947	967
$T_{\text{B\&K}} (^{\circ}\text{C})$	912	952	1065	995	969	921	948	892	918	950	937	971	958	933	927	912	852	858	949	908	936
$ \Delta T $	18	18	32	12	35	10	14	14	36	27	30	21	5	32	32	39	29	49	33	39	31

textures with abundant triple point grain–grain contacts (Fig. 3A, B). Under the scanning-electron microscope (SEM), mineral grains show no discernible chemical zoning (Fig. 3B). Most peridotite samples are unfoliated to weakly foliated. Where peridotite samples are strongly foliated, the fabric is typically defined by spinel and occasionally by pyroxene. A total of 5 samples show mineralogical banding manifest as bands of bright green chromium–diopside.

Although equilibrium textures dominate (Fig. 3A, B), some samples show signs of disequilibrium (Fig. 3C, D). These textures are most common in smaller samples (≤ 50 g) or near xenolith/lava contacts and appear to result from interactions with the higher-temperature host lava. The most common expression of this thermal disturbance is the development of sieve-textured coronas on apparently pristine orthopyroxene cores (Fig. 3C). In three samples orthopyroxene has reacted completely to become entirely sieve-textured; some orthopyroxene grains have developed coronas of clinopyroxene and olivine. Other disequilibrium features include the breakdown of spinel and the production of melt veinlets containing neoblasts of olivine (Fig. 3D). Similar textures have been interpreted by Shaw et al. (1998) as dissolution of orthopyroxene resulting from interaction between peridotite xenoliths and entraining lava. The experiments of Shaw et al. (1998) showed that orthopyroxene, when in contact with silica-undersaturated melts such as basanites, will dissolve incongruently to form olivine, clinopyroxene, and a Si-rich melt.

4. Analytical techniques

Mineral compositions were analysed using a fully automated CAMECA SX-50 electron microprobe (EMP) at the University of British Columbia. Operating conditions in the wavelength-dispersion mode included: excitation voltage, 15 kV; beam current, 10 nA; peak count time, 20 s; background count-time, 10 s; spot diameter, 10 μm . Data reduction was done using the PAP $\varphi(\rho Z)$ method (Pouchou and Pichoir, 1985).

Mineral chemical data were collected for all major phases in 44 samples: olivine (ol) orthopyroxene (opx), clinopyroxene (cpx), and spinel (sp) (Table 3). The compositions of coexisting pyroxenes were measured for geothermometric purposes. For each sample,

6 to 10 mineral pairs were analyzed, including several core and rim pairs to assess the extent of chemical zoning. Zoning was absent in all samples except in those showing strong disequilibrium textures. Temperature calculations were based on EMP analyses of adjacent orthopyroxene and clinopyroxene grains.

Olivine and pyroxene grains have compositions consistent with mantle peridotite; magnesium numbers ($\text{Mg\#} = \text{Mg}/(\text{Mg} + \text{Fe})$) for olivine, orthopyroxene and clinopyroxene vary between 0.887–0.917, 0.887–0.924, and 0.894–0.944, respectively. Spinel compositions are the most varied; the average chromium number ($\text{Cr\#} = \text{Cr}/(\text{Cr} + \text{Al})$) for spinel in peridotite is 0.352, but the range is 0.0181 (websterite) to 0.727 (Iherzolite).

5. Geothermometry

Two-pyroxene geothermometry, based on diopside and enstatite solubility in coexisting ortho- and clinopyroxene, provides a reliable means of estimating equilibrium temperatures in rapidly transported mantle rocks (e.g., Wood and Banno, 1973; Wells, 1977). The Brey and Köhler (1990) geothermometer [BK90] is a revised calibration of previous estimations of the two pyroxene thermometer (Wood and Banno, 1973; Wells, 1977) that accounts for more realistic pyroxene compositions. Temperatures calculated for the same mineral pairs using the Wells (1977) thermometer are consistently lower than BK90 temperatures below approximately 900 °C and higher than BK90 temperatures above approximately 980 °C (Table 3). We elected to use the BK90 thermometer because it is a more recent calibration and, thus, has been calibrated over a wider range of temperatures and mineral compositions.

The BK90 thermometer requires an assumption of pressure; our calculations assume a pressure of 12 kbar for all samples. Based on the temperature range of our sample suite, a pressure difference of about 5 kbar is estimated between the highest and lowest temperature xenoliths. When the lowest and highest temperature xenoliths are re-calculated using a 'corrected' pressure the corresponding temperature difference is ≤ 15 –20 °C; the inherent uncertainty (1σ) associated with the BK90 thermometer is ± 15 °C.

We collected EMP data on peridotite samples in batches. Our first batch contained 10 samples in which mineral compositions were measured and pro-

cessed; subsequent samples were analyzed in batches of 5. The geothermometry results were plotted sequentially in groups as acquired (Fig. 4). The goal of plotting the sequential distribution of temperatures was to ascertain when enough samples had been analysed to ensure that the full range of temperatures had been captured. We tracked this by plotting the running values of T_{\max} , T_{\min} and $T_{\max} - T_{\min}$ against the sequential sample number (Fig. 4). Plotted in this way we sought the situation where the value of $T_{\max} - T_{\min}$ no longer changed as new samples were processed. As shown in Fig. 4B, a constant value was reached between samples 25 and 30; additional data collection did not change the values of T_{\max} , T_{\min} or $T_{\max} - T_{\min}$. This analysis suggests that suites with fewer than 25–30 samples may not provide statistically valid limits on the temperature distribution in the lithospheric mantle. Conversely, we would argue that our suite of samples records the maximum and minimum temperatures of the mantle lithosphere sampled by the basanite magma. The ambient mantle temperatures from peridotite samples are also plotted in histogram format. The data define a bell-shaped curve that has the highest proportion of temperatures concentrated between 900 and 950 °C. The lowest concentration of temperatures is observed at the lowest and highest temperature extremes of the data set (i.e., 800–850 °C and 1050–1100 °C).

6. Results

Geothermometry results for all 44 xenoliths sampled are reported in Table 4 and shown graphically in Fig. 4. The minimum temperature calculated from our peridotite suite is 810 ± 26 °C. The maximum ambient mantle temperature is more difficult to constrain because some xenoliths have been thermally disturbed during transport. Samples with sieve-textured orthopyroxene grains generally give higher equilibration temperatures and greater variances; in some samples, sieve-textured rims provide temperatures up to 100 °C higher than apparently pristine cores (Fig. 4A). For these samples, the high-temperature rim analyses were not included as ambient mantle temperatures. Three samples with strong development of sieve-textured orthopyroxene record temperatures of 1100–1150 °C (Fig. 4B), which are interpreted as re-equilibration

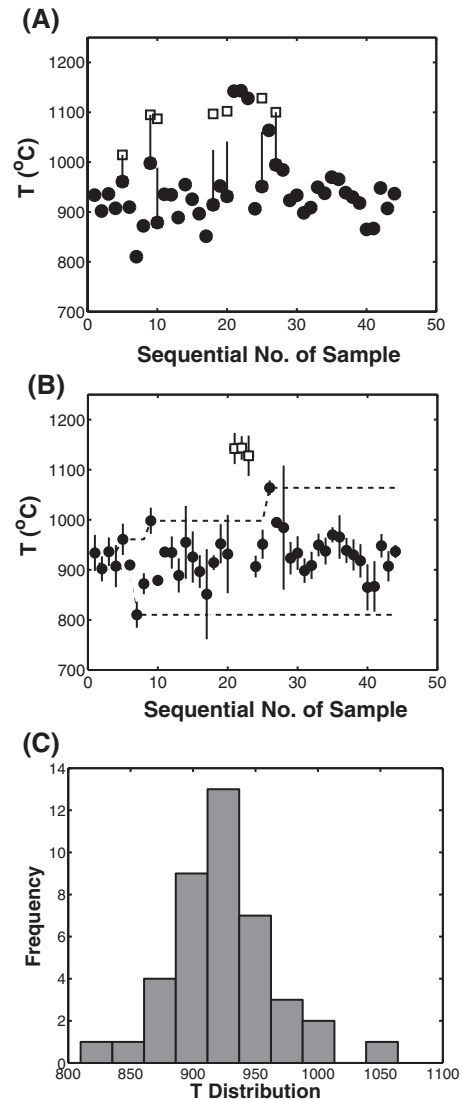


Fig. 4. Results of two-pyroxene geothermometry for 44 samples of peridotite (Brey and Kohler, 1990). (A) Mean temperature (°C) of each sample is plotted in the sequence that the data were collected. Dotted tie lines connect temperatures associated with equilibrium core (filled squares) and disturbed rim (open squares) compositions of minerals. (B) Distribution of ambient mantle temperatures illustrating the running maximum and minimum values recovered from the entire suite. Filled circles represent ambient mantle samples, open squares represent high temperature, thermally-disturbed samples (Fig. 3). The running maximum and minimum temperatures are used to determine when $T_{\max} - T_{\min}$ no longer changes (see text). (C) Histogram of ambient mantle temperatures collected from this peridotite suite based on a bin interval of 25 °C.

Table 4

Mineralogical, chemical, and thermal traits of all samples (MH-02-), including: weight, mineral modes and chemistry, and equilibration temperature (T_A : ambient samples; T_H : high – T_{rim} ; ΔT : $T_{max} - T_{min}$)

No.	Wt. (g)	Density (g/cm ³)	¹ Modes (%)				² Rock type:	X_{Fe}			Cr#		
			Ol	Opx	Cpx	Sp		Ol	Opx	Cpx	Sp	T_A	T_H
110*	369	3.24	59	23	16	2	Lh	0.899	0.088	0.071	0.11	934	
108*	2079	3.31	70	21	7	1	Lh	0.905	0.084	0.065	0.21	902	
111*	471	3.33	61	22	15	2	Lh	0.887	0.103	0.089	0.10	936	
10	196	3.17	60	20	18	2	Lh	0.901	0.091	0.079	0.14	907	
9c	156	3.27	58	30	10	2	Lh	0.916	0.075	0.059	0.52	961	1015
9b	50	3.26	65	30	3	2	Hx	0.915	0.075	0.050	0.56	910	
10b	40	3.24	58	30	10	2	Lh	0.913	0.078	0.043	0.25	810	
109b	21	3.23	60	30	8	2	Lh	0.912	0.075	0.051	0.49	872	
18b	53	3.24	60	30	8	2	Lh	0.915	0.074	0.057	0.59	998	1095
104*	411	3.33	75	17	6	1	Lh	0.913	0.079	0.054	0.21	879	1087
100*	1461	3.29	75	24	6	1	Hx	0.915	0.071	0.046	0.48	936	
115	48		70	25	3	2	Hx	0.916	0.071	0.043	0.47	935	
122*	593	3.30	63	21	13	3	Lh	0.895	0.090	0.065	0.13	889	
117	54	3.18	70	20	8	2	Lh	0.912	0.072	0.045	0.47	955	
5b	81		77	17	4	2	Hx	0.916	0.067	0.046	0.52	926	
8b	161		73	22	3	2	Hx	0.906	0.075	0.052	0.42	897	
4A	48	3.21	65	24	8	3	Lh	0.910	0.074	0.043	0.32	851	
9d	16		65	23	10	2	Lh	0.907	0.073	0.052	0.16	914	1097
10c	22	3.23	62	33	3	2	Hx	0.914	0.069	0.044	0.45	952	
10d	22	3.13	71	20	7	2	Lh	0.907	0.080	0.054	0.12	931	1102
15	63	3.25	60	30	8	2	Lh	0.907	0.082	0.058	0.18	907	
21	40		65	23	10	2	Lh	0.907	0.080	0.064	0.17	951	1128
109	237		70	21	7	2	Lh	0.915	0.069	0.057	0.42	1064	
112*	245		75	22	2	1	Hx	0.912	0.072	0.050	0.51	995	1100
124	1036		0	40	45	15	We	–	0.108	0.092	0.02	984	
20	329	3.25	65	18	15	2	Lh	0.903	0.080	0.061	0.21	923	
19*	578	3.24	79	17	2	1	Hx	0.915	0.065	0.037	0.46	933	
102	184		60	24	15	1	Lh	0.903	0.084	0.059	0.17	898	
113*	366		79	17	2	1	Hx	0.915	0.074	0.046	0.53	909	
114*	374	3.23	79	17	3	1	Hx	0.917	0.071	0.049	0.52	950	
115b*	386	3.23	76	20	2	1	Hx	0.913	0.072	0.048	0.46	937	
116	256		66	25	8	1	Lh	0.917	0.065	0.047	0.52	970	
117b*	340	3.21	74	22	3	1	Hx	0.913	0.071	0.049	0.47	966	
118*	215		76	19	3	1	Hx	0.914	0.068	0.040	0.80	939	
119	297	3.19	62	34	2	2	Hx	0.914	0.069	0.044	0.41	930	
120*	621	3.33	78	19	2	1	Hx	0.915	0.074	0.049	0.50	918	
121*	2830	3.34	67	23	8	2	Lh	0.905	0.081	0.053	0.17	865	
123*	981	3.25	68	22	8	2	Lh	0.903	0.085	0.057	0.20	867	
125*	298		79	18	2	1	Hx	0.911	0.077	0.051	0.44	948	
95LM1*	3385	3.31	75	20	3	2	Hx	0.917	0.071	0.045	0.51	907	
19b*	304	3.24	72	24	3	1	Hx	0.911	0.074	0.053	0.46	937	
12b	21		60	29	8	3	Lh	0.909	0.078	0.064	0.48		1142
12	137	3.20	60	29	8	3	Lh	0.906	0.078	0.063	0.17		1143
12(2)	137	3.20	70	26	3	1	Hx	0.904	0.084	0.070	0.16		1128

¹ Olivine (Ol); orthopyroxene (Opx); clinopyroxene (Cpx); spinel (Sp).

² Lherzolite (Lh); harzburgite (Hx); websterite (We).

*Modes calculated using the Rietveld technique (Rietveld, 1967; Raudsepp et al., 1999).

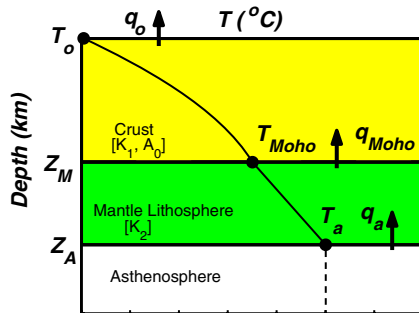


Fig. 5. Schematic representation of model for conductive heat transfer in the crust and mantle lithosphere. Variables include: temperature and heat flow at the Earth's surface (T_0 , q_0), at the MOHO (T_{moho} , q_{moho}), and at the top of the asthenosphere (T_a , q_a), thermal conductivity and heat production in the crust (K_1 , A_0) and mantle lithosphere (K_2), and the depths to the MOHO ($Z_M=36$ km) and the top of the asthenosphere (Z_A). Heat production in the mantle lithosphere is assumed negligible.

temperatures approaching the lava temperature. The maximum ambient temperature of this sample suite is 1065°C with a sample variance of 15°C . In summary, these temperatures provide the minimum (810°C), maximum (1065°C), and total temperature difference ($>255^\circ\text{C}$) recorded by samples of peridotite mantle from beneath Llangorse Mountain. The temperature difference ($T_{\text{max}} - T_{\text{min}}$) relates directly to the minimum thickness of the mantle lithosphere; the exact value (e.g., thickness) depends on the geothermal gradient assumed.

7. Model of the lithospheric mantle

Our ultimate goal is to constrain the thermal state of the lithosphere underlying the northern Canadian cordillera by combining petrological information gathered from mantle-derived peridotite xenoliths with simple models for conductive heat flow in the lithosphere. The basis of our model lithosphere for the northern Cordillera is summarized in Fig. 5 and comprises a crust of specified thickness (Z_M) and a constant surface temperature (T_0) and surface heat flow (q_0). Seismic reflection data, collected as part of the Lithoprobe program (Clowes et al., 1999), is used to define the depth to the MOHO in the northern Cordillera (transect line 22; Hammer et al., 2000; Hammer and Clowes, 2004). Beneath the Atlin region, the MOHO depth is estimated to be 36 km (Z_M ; Hammer

and Clowes, 2004). The crustal layer has a specific range in heat production (A_0) values and a constant thermal conductivity (K_1) and overlies a mantle lithosphere having a uniform thermal conductivity (K_2) and no heat production. The crustal layer is assumed to have an exponential distribution of heat producing elements. Heat transfer in the mantle lithosphere is purely conductive. The depth to the base of the mantle lithosphere (Z_A) is unknown but is taken as marking the top of the convecting asthenospheric mantle. Our aim is to investigate the temperatures and heat fluxes at the two major boundaries in this schematic model (e.g., T_{moho} , q_{moho} , T_a and q_a).

The research efforts of Hyndman and Lewis (1999), Lewis et al. (2003), and Hyndman et al. (in press) have provided bounding estimates on the values of surface heat flow (q_0) and crustal heat production (A_0) for the northern Cordillera (Table 5). Much of their work has been directed at explaining heat flow variations between the Cordillera and the North American craton to the east. We have used their results to set some of the geophysical properties for the crust (e.g., Fig. 5) by adopting values that are most relevant to the northern Canadian Cordillera at latitudes consistent with Atlin, British Columbia (Table 5). Readers are directed to Hyndman and Lewis (1999) and Lewis et al. (2003) for detailed discussions of the acquisition, distribution and quality of the heat flow data.

Table 5

Physical parameters used in geotherm models (see text)

Property	Layer 1	Layer 2	Layer 3
	Crustal lithosphere	Mantle lithosphere	Asthenosphere
T_0 [$^\circ\text{C}$]	10	–	–
q_0 [mW m^{-2}]	76 ± 14	–	–
Z_{moho} [km]	36	–	–
T [$^\circ\text{C}$] xenolith ^a	800–850		
T [$^\circ\text{C}$] xenolith ^b		1050–1100	
A [$\mu\text{W m}^{-3}$]	1.6 ± 0.8	0	0
K [$\text{W m}^{-1} \text{K}^{-1}$]	2.5	3.2	3.2
ρ [kg m^{-3}]	2700	3300	3300
α [K^{-1}]	–	–	$3.0\text{E}-5$
κ [$\text{m}^{-2}\text{s}^{-1}$]	–	–	$1.0\text{E}-6$
η [Pa s]			$10^{19.4}$

^a Range of minimum temperatures recovered from mantle peridotite samples.

^b Range of maximum temperatures recovered from mantle peridotite samples.

7.1. Surface heat flow

Relative to the Canadian craton, the Cordillera is characterized by high surface heat flow (Hyndman and Lewis, 1999). Recent work by Lewis et al. (2003) has provided a series of new measurements showing that surface heat flow across the entire northern Cordillera is approximately twice as high as observed in the craton (80–100 versus 40–60 mW m⁻², respectively). In addition, there are differences in q_0 between domains north and south of 59°N latitude, and between different tectonic belts (i.e., Intermontane Belt versus Omineca Belt). The Llangorse volcanic field is situated entirely within the Intermontane Belt (Aitken, 1959). Thus, we have used heat flow values that represent the average values from across the Intermontane Belt. The range of heat flow values in the Intermontane Belt is 58–98 mW m⁻², with an average of 76 ± 14 mW m⁻² (1σ) (Table 5).

7.2. Heat production

Lewis et al. (2003) provide new measurements of radiogenic heat production in crustal rocks across the northern Cordillera. Crustal rocks, especially younger intrusions situated in the northernmost portion of the Cordillera (59–64°N) within the Omineca Belt, have substantially higher values of heat production than similar rocks exposed between 57–59°N or within the Intermontane Belt. The geological units to the north of 59°N have a mean heat production of 4.6 ± 2.4 versus 1.6 ± 0.8 $\mu\text{W m}^{-3}$ for rocks south of 59°N. For the purposes of our modeling, we have used the latter range of heat production values (e.g., south of 59°N) which is also close to the average heat production value for the Intermontane Belt as a whole (1.15 ± 1.27 $\mu\text{W m}^{-3}$). Lewis et al. (2003) used these data to argue that the exceptionally high heat flow observed for the Cordillera north of 59°N is largely due to the unusually high heat production of near-surface crustal rocks rather than higher temperatures at the base of the crust.

7.3. Lower crust temperatures

For the northern Canadian Cordillera between 57°N and 64°N, a reduced heat flow of 59 mW m⁻² is predicted (although there is very little heat generation

data between 57–59°N), which is similar to values predicted for the southern Canadian Cordillera (49–53°N) (Hyndman and Lewis, 1999; Lewis et al., 2003; Hyndman et al., in press). Depending on the model parameters adopted, Lewis et al. (2003) suggest a MOHO temperature (T_{moho}) of $825\text{--}950 \pm 100$ °C. Lewis et al. (2003) also used the values of compressional seismic wave velocities at the MOHO (e.g., Pn) to estimate the temperatures at the MOHO for the northern Cordillera using the strong negative correlation between Pn seismic wave velocities and apparent MOHO temperature developed by Black and Braile (1982). Adopting the Pn wave velocities for the northern Cordillera reported by Hammer et al. (2000; e.g., 7.8–7.9 km s⁻¹), they estimate a T_{moho} for the northern Cordillera of 800–1000 °C.

Our suite of mantle xenoliths provides a means of constraining the value of T_{moho} via geothermometry. Our rationale is that the coolest temperature recovered from the suite represents the shallowest mantle sampled by the magma and that the shallowest mantle should be coincident with the MOHO (Table 6). There is always the possibility that another sample, having a lower temperature, exists but it was not sampled by the basanite magma, or was not collected in the field, or was not prepared by us for EMP analysis. However, given our extensive thermometric database for this single locality, we suggest that our minimum temperatures (800–850 °C) are fair estimates of the temperature at the top of the mantle lithosphere and base of the crust (e.g., T_{moho}).

7.4. Crustal and mantle lithosphere

The steady-state conductive temperature distribution for the one-dimensional crustal lithosphere discussed above is given by:

$$T(z) = T_0 + \frac{q_0 z}{K_1} + \frac{A_0 Z_M^2}{K_1} \left(1 - \frac{z}{Z_M} - e^{-\frac{z}{Z_M}} \right) \quad 0 < z < Z_M \quad (1)$$

where K_1 is a constant and q_0 and A_0 have a preferred range of values based on Lewis et al. (2003). For each pair of values of q_0 and A_0 there will be a unique crustal geotherm that predicts unique, but correlated, values of T_{moho} and reduced heat flow (q_r). Fig. 6A illustrates the relationship between surface heat flow and crustal heat production embedded in Eq. (1). The lightly shaded box (Fig. 6A) denotes the range of

Table 6
Summary of model results

T_{moho} [°C]	800		850	
A_0	0.8	2.4	0.8	2.4
q_0 [mW m ⁻²]	65.5	86.6	68.9	90
q_{moho} [mW m ⁻²]	47.3	32	50.7	35.6
(dT_1/dZ) [°C km ⁻¹]	18.9	12.8	20.3	14.2
q_A [mW m ⁻²]	47.3	32	50.7	35.6
Z_A [km] at 1300 °C	70	86	64	76
	$T_A = 1100$ °C		$T_A = 1100$ °C	
Z_A [km]	56	66	52	59
ΔZ_{ML} [km] ^a	20	30	16	23
	Convection conditions			
ΔT [°C] ^b	292	231	304	246
$\log \eta$ (T_{ave}) ^c	19.41	19.51	19.39	19.48
T_{ave} [°C] ^d	1246	1216	1252	1223
T_{∞} [°C] ^e	1392	1331	1405	1347
D [km] ^f	44	52	43	50

^a Thickness of mantle lithosphere.

^b Minimum critical difference in temperature for convection.

^c Implied viscosity of convecting mantle given average temperature of layer.

^d Average temperature in convecting boundary layer.

^e Temperature at top of asthenosphere.

^f Minimum critical thickness required for convection.

values of q_0 and A_0 observed for the northern Cordillera near Atlin, B.C. The dashed lines are contours of reduced heat flow ($q_r = q_{\text{moho}}$) for all possible crustal geotherms; the contours show the specific values of reduced heat flow dictated by the range of observed surface heat flow and heat production values. Each geotherm also dictates a unique value of T_{moho} . However, our geothermometry on mantle peridotites constrains the value of T_{moho} to between 800 and 850 °C. By fixing the value of T_{moho} , the range of possible values of q_0 and A_0 are severely restricted (solid lines, Fig. 6A) and described by:

$$q_0 = 0.3679 Z_{\text{moho}} A_0 + \frac{[T_{\text{moho}} - T_0] K_1}{Z_{\text{moho}}}. \quad (2)$$

Combining the T_{moho} constraints with the restricted range of values of q_0 and A_0 (Fig. 6A; Lewis et al., 2003) greatly limits the range of model crustal geotherms (Fig. 6B). The complete solution space is denoted by the dark shaded quadrilateral in Fig. 6A which also defines the range of possible values of q_{moho} . For a fixed T_{moho} of 800 or 850 °C the values of reduced heat flow vary from 32 to 47 and 36 to 51

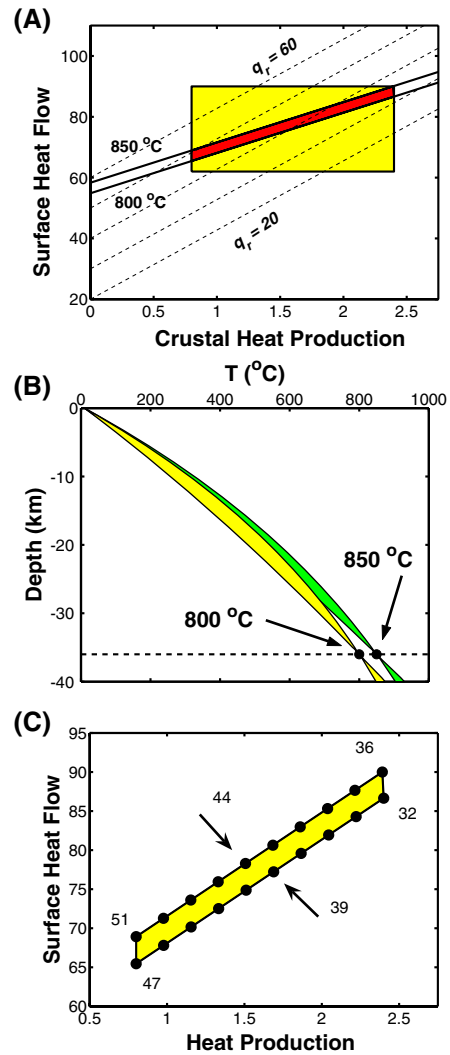


Fig. 6. Model results for temperature distributions in the crust. (A) The full range of values for surface heat flow (q_0 ; mW m⁻²) and crustal heat production (A_0 ; $\mu\text{W m}^{-3}$) consistent with T_{moho} values of 800 or 850 °C (solid lines). Corresponding model values of reduced heat flow q_r are contoured as dashed lines. Range of values of q_0 and A_0 reported for the northern Cordillera (Lewis et al., 2003) are represented by light grey box. Thus, the dark shaded field shows the restricted combination of values of q_0 and A_0 that are simultaneously consistent with the measurements of Lewis et al. (2003) and values of T_{moho} of 800 or 850 °C. (B) The family of feasible geotherms generated for the crustal lithosphere assuming values of T_{moho} of 800 or 850 °C. (C) The feasible solution space shown in A (dark grey shaded box) is expanded and labeled in terms of corresponding values of reduced heat flow. The solution space is defined by the intersection of the two solid lines (model) and the light grey shaded box (observed) in A.

mW m^{-2} , respectively (Fig. 6C; Table 6). In general, higher values of T_{moho} dictate higher values of reduced heat flow; this has substantial implications for the temperature distributions in the mantle lithosphere and ultimately the depths to the thermally controlled base of the lithosphere (e.g., Hyndman et al., in press).

The lithospheric mantle (e.g., Layer 2; Fig. 5) is coupled to the crust by the MOHO temperature and the reduced heat flow (Fig. 6B, C). The expected steady-state temperature distribution is described by:

$$T(z) = T_{\text{moho}} + \frac{[q_0 - 0.6321A_0Z_M]}{K_2} [z - Z_M] \quad Z_M < z < Z_A. \quad (3)$$

The total thickness of the mantle lithosphere is not known a priori, but we can rearrange Eq. (3) to explore the two unknowns: the depth to the asthenosphere (Z_A) and the temperature at that transition (T_A):

$$T(z) = \frac{q_{\text{moho}}}{K_2} Z_A + \left\langle T_{\text{moho}} - \frac{q_{\text{moho}}}{K_2} Z_M \right\rangle. \quad (4)$$

The distribution of model geotherms for the mantle lithosphere is shown in Fig. 7A for two different values of T_{moho} . The higher values of reduced heat flow associated with the 850 °C MOHO support higher geotherms and a potentially thinner mantle lithosphere. For example, if the 1300 °C isotherm was arbitrarily adopted as the thermally controlled base of the lithosphere, then the model geotherms using $T_{\text{moho}} = 800$ °C would indicate depths to the asthenosphere ($Z_{A, 1300}$) of 70–86 km versus 64–76 km for $T_{\text{moho}} = 850$ °C (Table 6). Conversely, a cooler MOHO implies a deeper boundary to the asthenosphere (Fig. 7B).

We propose an alternative constraint on the thickness of mantle lithosphere underlying this portion of the northern Cordillera based on the maximum temperatures recovered from our suite of mantle peridotite xenoliths (T_A ; Table 4). The maximum temperature clearly associated with ambient mantle lithosphere is close to 1100 °C and weakly disturbed samples record temperatures as high as 1150 °C (Table 4). The maximum xenolith temperatures are indicative of the hottest and deepest portions of the mantle lithosphere and provide estimates of the minimum thickness of mantle lithosphere (Fig. 7A). Clearly, the higher the temperatures of ambient mantle recovered from the xenoliths, the thicker the mantle lithosphere.

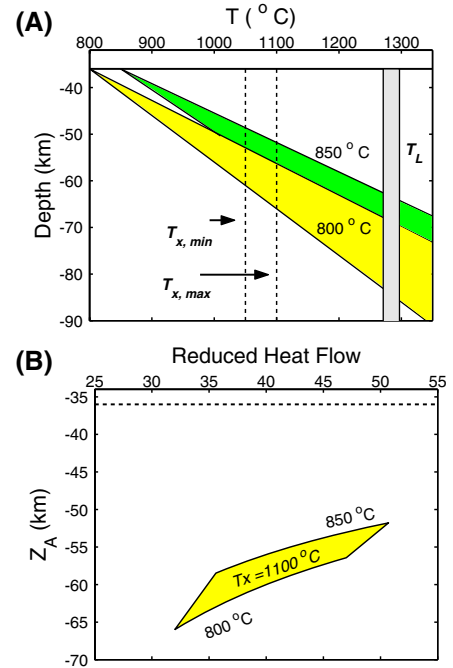


Fig. 7. Model geotherms for mantle lithosphere underlying the northern Canadian Cordillera. (A) Model temperature of mantle lithosphere plotted against depth (km); model geotherms are for T_{moho} values of 800 °C (light shading) and 850 °C (dark shading). Vertical dashed lines indicate the range of maximum temperatures (1050–1100 °C) recovered from peridotite xenoliths. (B) The same array of geotherms is represented as values of reduced heat flow (q_{moho}) and depth to the asthenosphere (Z_A) assuming T_A of 1100 °C and fixed values of T_{moho} (800 and 850 °C; see Table 6).

The range of implied depths to the base of the mantle lithosphere (Z_A) are explicitly mapped out in terms of T_{moho} and the maximum xenolith temperature (T_A) in Fig. 7B. The thickest mantle lithosphere (56–66 km) is supported by the coolest T_{moho} and higher values of T_A ; the thinnest lithosphere (52–59 km) is associated with high values of T_{moho} and lower values of T_A (Table 6).

8. Discussion

8.1. Crustal geotherms

We have used petrological information recovered from mantle-derived peridotite xenoliths in combina-

tion with steady-state conductive heat transfer arguments to create a model set of geotherms for the lithosphere underlying the northern Cordillera. These geotherms define the thermal state of the lithosphere and there are attendant petrological implications. Firstly, the high MOHO temperatures implied by the coolest mantle peridotite temperatures demand elevated crustal geotherms. Conventional crustal geotherms usually indicate lower MOHO temperatures (e.g., 400–500 °C) and have paths that lie well within the kyanite stability field (Fig. 7A). The model geotherms for the northern Cordillera describe paths that, at depth, become tangential to the kyanite–sillimanite univariant curve. Kyanite remains the most likely stable aluminosilicate in pelitic lower crustal rocks; however, small thermal perturbations could easily allow for development of sillimanite. If the MOHO were any hotter (e.g., ~900 °C), then sillimanite would be the stable phase at the base of the crust and there would be a kyanite–sillimanite isograd within the lower portion of the crustal column. This is significant as the higher geotherm in the northern Cordillera implies that high-temperature mineral suites, perhaps even sillimanite, will be stable in the lower crust.

The elevated crustal geotherm requires consideration of partial melting of crustal rocks. For the purposes of discussion we have plotted the water-saturated and dry solidi for mafic crustal rocks (gabbro; Lambert and Wyllie, 1972) against the model geotherms (Fig. 8). Melting of gabbro would only proceed under conditions of full water saturation and such conditions are unlikely to be met in the deep crust. Granitoids with lower melting points could perhaps be induced to melt, but these rocks are more likely to be concentrated in the upper to middle crust where temperatures are substantially lower. If any melting has occurred in the lower crust, it is most likely to have occurred at water-undersaturated conditions that might attend metamorphic dehydration reactions (e.g., breakdown of muscovite, biotite or hornblende; Whitney, 1988; Patino-Douce et al., 1990).

8.2. Lithosphere–asthenosphere transition

We have used the maximum xenolith temperatures as estimates of the temperature at the base of the

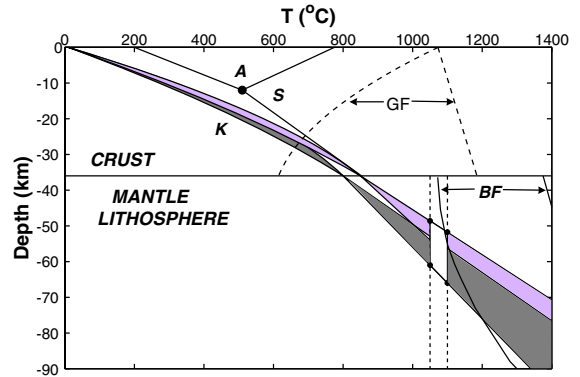


Fig. 8. Model geotherms for the combined crustal and mantle lithosphere. Model geotherm temperatures are plotted against depth (km) and compared to stability fields of common metamorphic minerals (K: kyanite; S: sillimanite; A: andalusite; Holdaway, 1971), anhydrous (high temperature curve) and hydrous (low temperature curve) solidi for gabbro (GF; Lambert and Wyllie, 1972). Conductive mantle lithosphere geotherms terminate against maximum temperatures from mantle xenoliths (1050–1100 °C; solid dots) defining a quadrilateral in T – Z space containing the minimum depth (and temperature) to the convective mantle asthenosphere. Also shown are experimentally determined liquidus curves from Orlando et al. (2000; <1 wt.% total volatiles) and from Jakobsson and Holloway (1986; 4.0–4.5 wt.% total volatiles). These curves define the basanite melt field (BF), which is constrained at high temperatures by the nearly-anhydrous basanite of Orlando et al. (2000) and at low temperatures by the hydrous basanite of Jakobsson and Holloway (1986).

mantle lithosphere; the implication is that the hotter asthenospheric mantle underlying this boundary is capable of sustained convection. The highest temperature xenoliths suggest that the base of the mantle lithosphere is close to 1100 °C. Cooler MOHO temperatures (800 °C) suggest values of q_A between 32.0 and 47.3 (Table 6), whereas a hotter MOHO (e.g., 850 °C) requires higher mantle heat flow values (35.6–50.7; Table 6).

We use the heat flow calculated in the mantle lithosphere to investigate whether the minimum conditions for convection are met in the underlying asthenosphere. The problem is summarized as a layer of asthenosphere of unknown thickness (D) being heated from below and ultimately conducting all heat (q_A) into the base of the mantle lithosphere (Fig. 9; after Turcotte and Schubert, 2002, and Poirier, 2000). The heat flow (q_A) into the base of the lithosphere is equivalent in magnitude to the MOHO heat flow (q_{moho}) because of the lack of heat sources

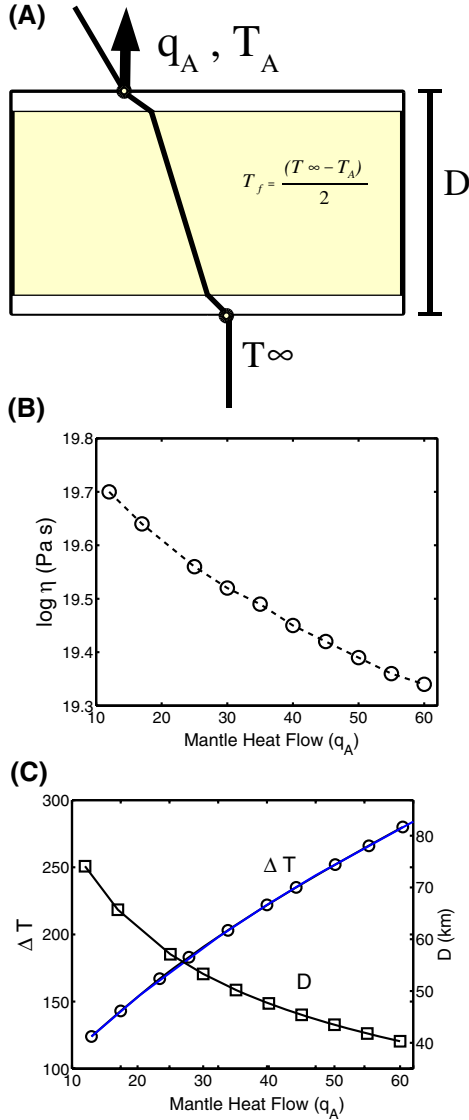


Fig. 9. (A) conceptual model for convective instabilities in a layer of asthenosphere being heated from below (see text); (B) Calculated viscosity in heated layer; (C) The ΔT and the value of D implied by range of heat flow values ($q_r = q_A$) for the Cordilleran mantle lithosphere.

and sinks in the mantle lithosphere. Our question concerns the rise of convective instabilities in a layer of asthenosphere as it is heated from below: given the observed mantle heat flow (q_A), under what conditions will convection in the underlying layer be sustained?

The Nusselt number (Nu ; Poirier, 2000) is a measure of convective heat flow across the layer ratioed to the heat flow that conduction would transport:

$$Nu = \frac{q_A D}{K_2 [T_A - T_\infty]}. \quad (5)$$

The convecting layer is partially defined by a temperature difference (ΔT) between the cool top (T_A) and hotter bottom (T_∞) (Fig. 9). Where $Nu < 1$, heat transfer is dominantly by conduction; conversely, convection requires $Nu > 1$. The Rayleigh number (Ra) measures the relative importance of buoyancy forces favouring convection versus the viscous drag forces hindering convection:

$$Ra = \frac{\rho g \alpha [T_A - T_\infty] D^3}{\eta \kappa} \quad (6)$$

where α is thermal expansivity, κ is thermal diffusivity, and η is the viscosity of the convecting fluid (Tables 5 and 6; Fig. 9A). Theory and experimentation show the Nu number to be proportional to the Ra number to the one-third power as given by:

$$Nu = 0.225 Ra^{1/3} \quad (7)$$

(Turcotte and Schubert, 2002). Rearranging Eq. (7) allows us to write an expression relating the mantle heat flow (q_A) to a set of physical constants for the layer of asthenosphere and the temperature difference across that layer (ΔT):

$$q_A = 0.225 K_2 \left[\left\langle \frac{\rho g \alpha}{\kappa} \right\rangle^{1/3} \right] \frac{\Delta T^{4/3}}{\eta^{1/3}}. \quad (8)$$

Specifically, Eq. (8) relates the reduced heat flow ($q_r = q_A$) to the minimum critical temperature difference needed to sustain convection in the underlying asthenosphere. We treat the viscosity of the fluid as a constant but allow its value to reflect the average and unknown temperature of the convecting layer ($T_f = 0.5 * [T_A + T_\infty]$). The viscosity of the mantle is approximated by the rheology of wet dunite (e.g., Chopra and Paterson, 1981; Dixon et al., 2004) and the temperature dependent function is:

$$\ln \eta = \frac{11505}{T_f (^\circ\text{C})} + 35.45. \quad (9)$$

The results of these calculations are summarized in Fig. 9B and C and Table 6. The known values include

the heat flow (q_A) and the temperature (1100 °C) on the upper boundary representing the base of the mantle lithosphere. The higher the mantle heat flow, the lower the viscosity of the mantle layer needed for convection (Fig. 9B). The viscosity of the convecting mantle is calculated by this method to be approximately $10^{19.4}$ Pa s (Fig. 9B). Values of ΔT increase with increasing mantle heat flow and, for our range of q_A , we calculate values of 231 to 304 °C (Fig. 9C; Table 6). The minimum critical thickness of the convecting layer (D) decreases with increasing mantle heat flow (Fig. 9C).

Our incorporation of xenolith temperature data into simple geotherm models suggests a mantle lithosphere extending to depths of 52–66 km depth depending on the temperature of the MOHO (Table 6; Fig. 10). This corresponds with a mantle lithosphere as thin as 16 km or as thick as 30 km (Table 6). Over this depth interval the mantle lithosphere comprises only spinel peridotite (Fig. 10; Robinson and Wood, 1998), rather than garnet-bearing peridotite, which is consistent with the petrography of all peridotites recovered from Llangorse. The convect-

ing asthenospheric mantle would have an average viscosity of $10^{19.4}$ Pa s, average temperatures of between 1210 and 1255 °C, and minimum temperatures towards the base of the convecting layer would be 1330–1405 °C (Fig. 10; Table 6). The minimum critical thickness of the convecting mantle layer varies between 43 and 52 km.

8.3. Implications for NCVP magmatism

The lithospheric mantle in the northern Canadian Cordillera has been studied indirectly by geophysical crustal-scale surveys (Clowes et al., 1999; Hyndman and Lewis, 1999; Hammer et al., 2000; Snyder et al., 2002; Lewis et al., 2003; Hammer and Clowes, 2004) and directly via studies of mantle-derived xenoliths from volcanic rocks (Nicholls et al., 1982; Francis and Ludden, 1995; Shi et al., 1998; Peslier et al., 2000a,b). Here, we summarize previous models advanced for the lithospheric mantle in the northern Cordillera and compare them to our preferred model.

Fig. 11A illustrates the model lithosphere from Nicholls et al. (1982), based on their studies of alkaline basalts and peridotite xenoliths from across the southern and central Canadian Cordillera. They showed that the lavas could not be partial melts of the xenoliths they carried, but were derived from a deeper source. Peridotite xenoliths were interpreted as sourcing from the lithospheric mantle and the lavas as deriving from the underlying 'low velocity zone' (e.g., asthenospheric mantle). They suggested a depth to the 'low velocity zone' of between 45 and 100 km, based on seismic data. They also used two-pyroxene thermometry (Wells, 1977) on peridotite xenoliths from many localities and showed that the peridotite xenoliths (recording temperatures of 900–1200 °C) equilibrated well below the peridotite solidus. An average geotherm was adopted based on observed heat flow (Pollack and Chapman, 1977) which implied a MOHO temperature of 765 °C at 36 km depth. The maximum xenolith temperature (1200 °C) on this geotherm predicts the asthenosphere/lithosphere boundary at 90 km (Eq. (3)). This estimate of the depth to the base of the lithosphere was shown to be consistent with the geophysical estimates of the low velocity zone (45–100 km).

Fig. 11B depicts the corresponding model of Francis and Ludden (1995) and Shi et al. (1998). Francis

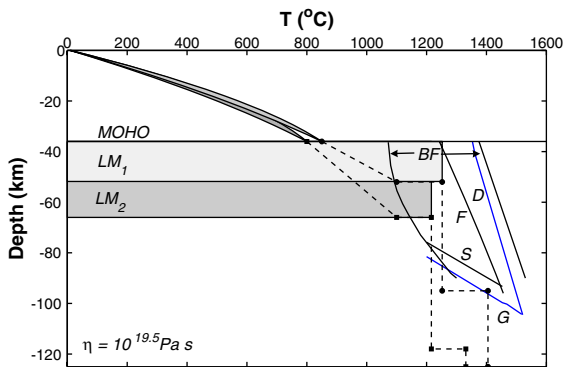


Fig. 10. Implications of model geotherms for thickness and temperature distributions in Cordilleran mantle lithosphere. Coolest and hottest mantle lithosphere geotherms terminate at depths of 66 km (LM_2) and 52 km (LM_1), respectively. Other reference curves include the solidi (heavy lines) for fertile (F: Hirschmann, 2000) and depleted (D: Robinson and Wood, 1998) peridotitic mantle, and the approximate positions of the corresponding spinel (S)/garnet (G) transition for each peridotite (after Robinson and Wood, 1998). Calculated temperatures in convecting mantle asthenosphere (dashed lines with filled circles or squares) are consistent with an average mantle model viscosity of $10^{19.5}$ Pa s (see Table 6). Basanite melt field (BF) is delimited by basanite liquidus curves for hydrous and anhydrous melts (see Fig. 8).

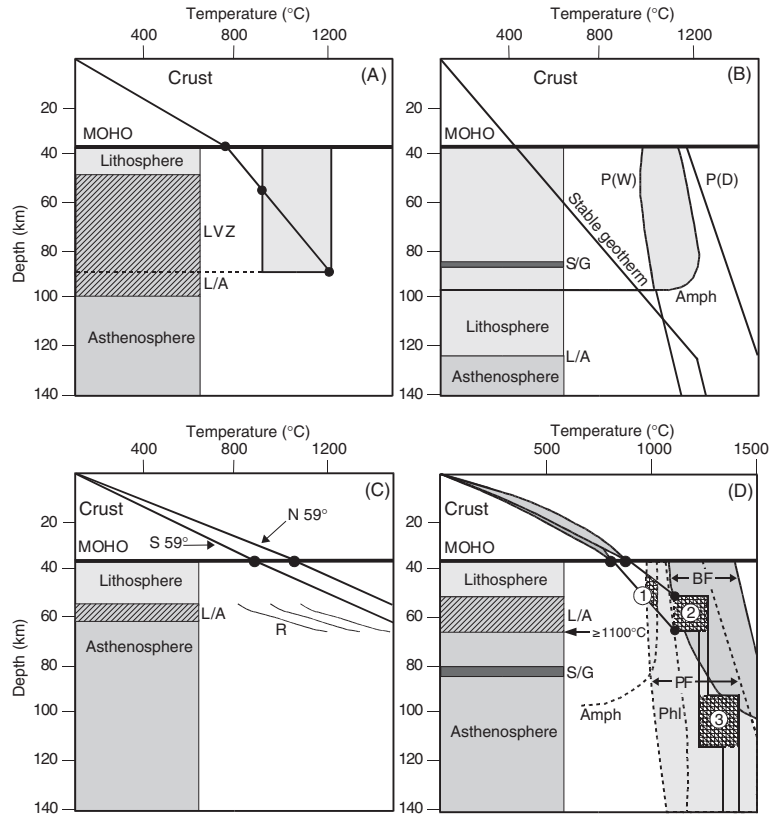


Fig. 11. Summary of models proposed for northern Canadian Cordillera lithosphere. (A) Nicholls et al. (1982) used equilibration temperatures for peridotite xenoliths from British Columbia (shaded box; 900–1200 °C) to suggest a $T_{\text{moho}} = 765$ °C and the lithosphere/asthenosphere boundary (L/A) at 90 km; the seismically defined low velocity zone (LVZ) is at 45–100 km for south-central BC. (B) Francis and Ludden (1995) and Shi et al. (1998), explored potential melting regions (shading) for dry (P(D)) and wet peridotite (P(W)); also shown is the melting curve for amphibole (Amph) and the spinel/garnet transition zone (S/G). (C) Compilation of geophysical work (Lewis et al., 2003; Hammer and Clowes, 2004; Hyndman et al., in press), showing two possible geotherms (for north and south of 59°N) and deep mantle reflectors (R; Hammer and Clowes, 2004). (D) Our preferred model for the northern Cordilleran lithosphere showing: i) a family of crustal geotherms consistent with T_{moho} values of 800–850 °C and our maximum xenolith temperature (1100 °C; Fig. 10), and terminating against the lithosphere/asthenosphere boundary (L/A) at depths of 52 and 66 km, respectively; ii) the peridotite melting field (PF, as shown in B), the basanite melt field (BF, Fig. 8), and the melting curves for amphibole (Amph) and phlogopite (Phl) (see dashed lines); iii) three potential zones of mantle melting (see numbers), including melting of: (1) mantle lithosphere within the amphibole stability field at shallow depths; (2) the base of the mantle lithosphere due to high temperatures sustained by the underlying asthenosphere; and (3) melting of the convecting, garnet-bearing asthenosphere.

and Ludden (1995) invoke the presence of amphibole in the source region of alkaline lavas in order to explain the trace chemistry patterns of some of the most primitive lavas observed in the NCVF (e.g., olivine nephelinites). Their model places the lithosphere/asthenosphere boundary considerably deeper than the amphibole stability field, and on this basis they argue that these lavas must source from the lithospheric mantle rather than the asthenospheric mantle. However, their lithosphere/asthenosphere

boundary is probably too deep for the active Cordillera and their geotherm is too cool, placing T_{moho} at too low a temperature (e.g., $T_{\text{moho}} = 400$ °C, rather than $T_{\text{moho}} > 800$ °C). Nevertheless, the possibility that alkaline lavas can be sourced from the lithospheric mantle is still valid. The source of the peridotite xenoliths is further constrained to be above the spinel/garnet transition (e.g., 80 km) due to the lack of textural or geochemical evidence of garnet (Shi et al., 1998).

An integrated geophysical model of the northern Cordilleran lithosphere, based on seismic and heat flow data, is summarized in Fig. 11C (Lewis et al., 2003; Hammer and Clowes, 2004; Hyndman et al., in press). The MOHO depth in this portion of the Cordillera is set at 35–36 km (Hammer and Clowes, 2004). Detailed studies of heat flow, heat generation, and crustal temperatures in the northern Cordillera (Lewis et al., 2003) are used to generate lithosphere geotherms and suggest MOHO temperatures of 800–1000 °C (Lewis et al., 2003) and 950 °C ± 100 °C (Hyndman et al., in press). Differences in crustal heat production result in slightly different crustal geotherms for areas north and south of 59°N latitude, with a slightly higher geotherm favoured for north of 59°N.

This integrated geophysical model suggests a lithosphere/asthenosphere transition between 50 and 60 km depth in the northern Cordillera, corresponding to a series of weak seismic reflectors within the upper mantle (Hammer and Clowes, 2004). Though not well constrained, these reflectors are located at approximately 60–75 km depth and dip at shallow angles to the northeast. These reflectors may result from heterogeneities in the mantle associated with the base of the lithosphere, as might arise from interleaving of lithospheric and asthenospheric material. Conversely, the heterogeneities may be related to partial melting processes. It is interesting to note that the depth of these mantle reflectors corresponds with the estimate of Hyndman et al. (in press) for the depth to the lithosphere/asthenosphere boundary.

Our model for the mantle lithosphere (Fig. 11D) underlying the northern cordillera is based on model geotherms constrained by the minimum (800–850 °C) and maximum (1100 °C) temperatures recovered from our peridotite xenolith suite. These geotherms are compared with other petrographic constraints to delimit the potential source regions for xenoliths and lavas. Experimentally determined basanite liquidus curves (see Fig. 8) from Orlando et al. (2000; <1 wt.% total volatiles) and Jakobsson and Holloway (1986; 4.0–4.5 wt.% total volatiles) define a basanite melt field (BF). Liquidus temperatures for melting of dry and wet peridotite (Hirschmann, 2000) define the region where melting of mantle material can occur (i.e., peridotite melting field (PF)). Superimposed on

this region are the melting curves of phlogopite (Phl) and amphibole (Amph) (Kushiro et al., 1968; Millhollen et al., 1974; Moderski and Boettcher, 1973), which define the stability limits of these hydrous minerals in the mantle. These constraints allow inferences to be made about the depth, temperature, and composition of the lithospheric mantle. The shaded column on the left of Fig. 11D shows our model depth to the lithosphere/asthenosphere boundary (L/A). Our model lithosphere is as thin as 16 km (L/A=52 km) or as thick as 30 km (L/A=66 km), depending on the geotherm used. We envision the base of the mantle lithosphere to be at a temperature ≥ 1100 °C, immediately underlain by a convecting asthenosphere comprising spinel-bearing peridotite; the depth to the spinel/garnet transition is estimated at >80 km (Robinson and Wood, 1998).

Our model supports three possible scenarios where melting of the mantle can occur. The first scenario involves melting of amphibole-bearing lithospheric mantle. Francis and Ludden (1995) interpret the geochemical diversity of nephelinite (± basanite) lavas as resulting from partial melting of amphibole-bearing peridotite (e.g., lithospheric mantle; Fig. 11B). Melting scenario 1 shows the restricted region in which this could occur. Given our model geotherms, amphibole is only stable in the mid-levels of the mantle lithosphere and should be absent at the base of the lithosphere. Thus, the Francis and Ludden (1995) model is possible only if melting occurs in the middle of the mantle lithosphere. However, temperatures at these depths are at least 100 °C below the basanite melt field (BF; Jakobsson and Holloway, 1986; Orlando et al., 2000). Scenario 1 is also too shallow to sample the deepest xenoliths observed at Llangorse Mountain. Scenario 2 involves melting of two potential sources: the base of the mantle lithosphere or the uppermost, spinel-bearing asthenosphere. Temperature gradients at the lithosphere/asthenosphere transition are high enough to bring the mantle temperature well into the basanite melting field. Scenario 3 allows for partial melting of the deep asthenosphere in the garnet stability field. Temperatures in scenario 3 lie well within the range of the basanite melt field and the garnet-bearing asthenosphere would easily melt during convective ascent. The model geotherm associated with the highest

Moho temperatures (i.e., 850 °C) would allow for basanite melts (hydrous) from as deep as 100 km. Previous workers (e.g., Francis and Ludden, 1990, 1995; Shi et al., 1998; Abraham et al., 2001) have argued that there is a conventional ‘garnet signature’ in trace chemistry of some NCVP lavas, suggesting a garnet-bearing asthenospheric source region. However, the model lithosphere presented by Francis and Ludden (1995) (Fig. 11B) also requires amphibole in the source region; these two requirements cannot be reconciled in our model. In addition, recent improvements in our understanding of the spinel/garnet transition indicate that this transition occurs much deeper than originally thought (Robinson and Wood, 1998; Klemme and O’Neill, 2000), calling into question the validity of the ‘garnet signature’. If the additional constraint of the garnet signature is lost, our model indicates that the garnet-bearing asthenosphere in the northern Cordillera is probably too deep to produce basanite melts. However, we cannot rule out a deep asthenospheric source for some NCVP lavas.

Our preferred interpretation is that the Llangorse Mountain lavas were produced by melting scenario 2 for the following reasons. Firstly, scenario 2 allows for sampling of the full mantle lithosphere as represented by the peridotite xenoliths at Llangorse Mountain (e.g., scenario 1 does not allow this). Secondly, unlike scenarios 1 and 3, two potential sources are involved (mantle lithosphere and asthenosphere). This could explain some of the chemical diversity observed in NCVP lavas (Edwards and Russell, 2000), in that more primitive melts (i.e., nephelinites and basanites) may source from the mantle lithosphere, whereas alkali-olivine basalts may have an asthenospheric source, as is traditionally proposed (e.g., Nicholls et al., 1982). Thirdly, scenario 2 is consistent with the rarity of garnet or amphibole-bearing peridotite xenoliths throughout the northern Cordillera (Littlejohn and Greenwood, 1974; Francis, 1976; Ross, 1983; Brearley and Scarfe, 1984; Nicholls et al., 1982; Shi et al., 1998). Furthermore, unlike melting zones 1 and 3, melting zone 2 lies well within the basanite liquidus melt region (Jakobsson and Holloway, 1986; Orlando et al., 2000), indicating that melting of the mantle at these temperature–pressure conditions could produce melts of the composition observed at Llangorse Mountain.

9. Conclusions

A refined model of the lithospheric mantle for the northern Canadian Cordillera is presented. This model combines both petrological and geophysical data and observations to create a series of model geotherms for this portion of the northern cordillera. The model geotherms place constraints on the temperatures (800–850 °C) and heat flow (32–51 mW m⁻²) at the base of the crust, as well as, the temperature and thickness of the Cordilleran mantle lithosphere. Our model indicates the minimum thickness of the lithospheric mantle to be between 16–30 km, corresponding to depths at the base of the lithosphere of 52–66 km. We consider three melting scenarios in the upper mantle; our preferred scenario involves melting at the base of the lithospheric mantle or uppermost asthenosphere, at depths of approximately 52–66 km and at temperatures between 1100–1300 °C.

Acknowledgments

Field work costs were borne by the Geological Survey of Canada through the Atlin Integrated Geoscience Project, courtesy of Bob Anderson. All other costs were met through NSERC via a Discovery Grant to J.K. Russell and a postgraduate scholarship to Margaret Harder. Our research was inspired through discussions with Ben Edwards, Phil Hammer, and Roy Hyndman and the final manuscript benefited substantially from thorough reviews by Dante Canil and Roy Hyndman.

References

- Abraham, A.-C., Francis, D., Polvé, M., 2001. Quaternary alkaline basalts as probes of the lithospheric mantle roots of the northern Canadian Cordillera. *Chemical Geology* 175, 361–386.
- Aitken, J.D., 1959. Atlin, British Columbia. Geological Survey of Canada, Memoir 307 (89 pp.)
- Black, P.R., Braile, L.W., 1982. Pn velocity and cooling of the continental lithosphere. *Journal of Geophysical Research* 87, 10557–10568.
- Brearley, M., Scarfe, C.M., 1984. Amphibole in a spinel lherzolite xenolith; evidence for volatiles and partial melting in the upper mantle beneath southern British Columbia. *Canadian Journal of Earth Sciences* 21, 1067–1072.

- Brearely, M., Scarfe, C.M., Fujii, T., 1984. The petrology of ultramafic xenoliths from Summit Lake, near Prince George, British Columbia. *Contributions to Mineralogy and Petrology* 88, 53–63.
- Brey, G.P., Köhler, T., 1990. Geothermobarometry in four-phase lherzolites: II. New thermobarometers, and practical assessment of existing thermobarometers. *Journal of Petrology* 31, 1353–1378.
- Canil, D., Brearely, M., Scarfe, C.M., 1987. Petrology of ultramafic xenoliths from Rayfield River, south-central British Columbia. *Canadian Journal of Earth Sciences* 24, 1679–1687.
- Carignan, J., Ludden, J., Francis, D., 1994. Isotopic characteristics of mantle sources for Quaternary continental alkaline magmas in the northern Canadian Cordillera. *Earth and Planetary Science Letters* 128, 271–286.
- Chopra, P.N., Paterson, M.S., 1981. The experimental deformation of dunite. *Tectonophysics* 78, 453–473.
- Clowes, R.M., Cook, F., Hajnal, Z., Hall, J., Lewry, J., Lucas, S., Wardle, R., 1999. Canada's LITHOPROBE Project (collaborative, multidisciplinary geoscience research leads to new understanding of continental evolution). *Episodes* 22, 3–20.
- Coney, P.J., Jones, D.L., Monger, J.W.H., 1980. Cordilleran suspect terranes. *Nature* 288, 329–333.
- Dixon, J.E., Dixon, T.H., Bell, D.R., Malservisi, R., 2004. Lateral variation in upper mantle viscosity: role of water. *Earth and Planetary Science Letters* 222, 451–467.
- Edwards, B.R., Russell, J.K., 1999. Northern Cordilleran volcanic province: a northern basin and range? *Geology* 27, 243–246.
- Edwards, B.R., Russell, J.K., 2000. Distribution, nature, and origin of Neogene–Quaternary magmatism in the northern Cordilleran volcanic province, Canada. *GSA Bulletin* 112 (8), 1280–1295.
- Edwards, B.R., Russell, J.K., Harder, M., 2003. An overview of Neogene to Recent volcanism in the Atlin volcanic district of the northern Cordilleran volcanic province, northwestern British Columbia. *Current Research. Geological Survey of Canada*. A6, 6 pp.
- Francis, D., 1976. The origin of amphibole in lherzolite xenoliths from Nunivak Island, Alaska. *Journal of Petrology* 17, 357–378.
- Francis, D., Ludden, J., 1990. The mantle source for olivine nephelinite, basanite, and alkaline olivine basalt at Fort Selkirk, Yukon, Canada. *Journal of Petrology* 31, 371–400.
- Francis, D., Ludden, J., 1995. The signature of amphibole in mafic alkaline lavas, and study in the northern Canadian Cordillera. *Journal of Petrology* 36, 1171–1191.
- Ghiorso, M.S., Sack, R.O., 1995. Chemical mass transfer in magmatic processes: IV. A revised and internally-consistent thermodynamic model for the interpolation and extrapolation of liquid–solid equilibria in magmatic systems at elevated temperatures and pressures. *Contributions to Mineralogy and Petrology* 119, 197–212.
- Hammer, P.T.C., Clowes, R.M., 2004. Accreted terranes of northwestern British Columbia, Canada: lithospheric velocity structure and tectonics. *Journal of Geophysical Research* 109, B03605, doi:10.1029/2003JB002749.
- Hammer, P.T.C., Clowes, R.M., Ellis, R.M., 2000. Crustal structure of NW British Columbia and SE Alaska from seismic wide-angle studies: coast plutonic complex to Stikinia. *Journal of Geophysical Research* 105, 7961–7981.
- Harder, M., Russell, J.K., in review. Basanite glaciovolcanism at Llangorse Mountain, northern British Columbia. *Bulletin of Volcanology*.
- Harder, M., Russell, J.K., Anderson, R.G., Edwards, B.R., 2003. Llangorse volcanic field, British Columbia. *Current Research. Geological Survey of Canada*. A6, 10 pp.
- Higgins, M.D., Allen, J.M., 1985. A new locality for primary xenolith-bearing nephelinites in northwestern British Columbia. *Canadian Journal of Earth Sciences* 22, 1556–1559.
- Hirschmann, M.M., 2000. Mantle solidus: experimental constraints and the effects of peridotite composition. *Geochemistry, Geophysics, Geosystems (G3)*, paper number 2000GC000070, 26 pp.
- Holdaway, M.J., 1971. Stability of andalusite and the aluminum silicate phase diagram. *American Journal of Science* 271, 97–131.
- Hyndman, R.D., Lewis, T.J., 1999. Geophysical consequences of the Cordillera-craton thermal transition in southwestern Canada. *Tectonophysics* 306, 397–422.
- Hyndman, R.D., Flück, P., Mazzotti, S., Lewis, T., Ristau, J., Leonard, L., in press. Constraints on current tectonics of the northern Canadian Cordillera. *Canadian Journal of Earth Sciences, SNORCLE volume*.
- Jakobsson, S., Holloway, J.R., 1986. Crystal–liquid experiments in the presence of a C–O–H fluid buffered by graphite+iron+wustite: experimental method and near-liquidus relations in basanite. *Journal of Volcanology and Geothermal Research* 29, 265–291.
- Klemme, S., O'Neill, H.St.C., 2000. The near-solidus transition from garnet lherzolite to spinel lherzolite. *Contributions to Mineralogy and Petrology* 138, 237–248.
- Kushiro, I., Syono, Y., Akimoto, S., 1968. Melting of a peridotite nodule at high pressures and high water pressure. *Journal of Geophysical Research* 73, 6023–6029.
- Lambert, I.B., Wyllie, P.J., 1972. Melting of gabbro (quartz eclogite) with excess water to 35 kilobars, with geological applications. *Journal of Geology* 80, 693–708.
- Lewis, T.J., Hyndman, R.D., Flück, P., 2003. Heat flow, heat generation, and crustal temperatures in the northern Canadian Cordillera: thermal control of tectonics. *Journal of Geophysical Research* 108 (B6), 2316, doi:10.1029/2002JB002090.
- Littlejohn, A.L., Greenwood, H.J., 1974. Lherzolite nodules in basalts from British Columbia, Canada. *Canadian Journal of Earth Sciences* 11, 1288–1308.
- Millhollen, G.L., Irving, A.J., Wyllie, P.J., 1974. Melting interval of peridotite with 5.7 percent water to 30 kilobars. *Journal of Geology* 82, 575–587.
- Moderki, P.J., Boettcher, A.L., 1973. Phase relationships of phlogopite in the system K₂O–MgO–CaO–Al₂O₃–SiO₂–H₂O to 35 kilobars: a better model for micas in the interior of the earth. *American Journal of Science* 273, 385–414.
- Monger, J.W.H., Price, R.A., Tempelman-Kluit, D.J., 1982. Tectonic accretion and the origin of the two major metamorphic and plutonic belts in the Canadian Cordillera. *Geology* 10, 70–75.

- Nicholls, J., Stout, M.Z., 1996. Basaltic lava flows and enclosed xenoliths as samples of the lithosphere and low velocity zone beneath northern British Columbia, a progress report. *Lithoprobe: Slave Northern Cordillera Lithospheric Evolution*, 50, pp. 109–115 (report).
- Nicholls, J., Stout, M.Z., 1997. Pressures and temperatures for ultramafic xenoliths, Atlin Lake area, British Columbia. *Lithoprobe: Slave Northern Cordillera Lithospheric Evolution*, 56, pp. 238–240 (report).
- Nicholls, J., Stout, M.Z., Fiesinger, D.W., 1982. Petrologic variations in Quaternary volcanic rocks, British Columbia, and the nature of the underlying upper mantle. *Contributions to Mineralogy and Petrology* 79, 201–218.
- Orlando, A., Conticelli, S., Armienti, P., Borrini, D., 2000. Experimental study on a basanite from the McMurdo Volcanic Group, Antarctica: inference on its mantle source. *Antarctic Science* 12, 105–116.
- Patino-Douce, A.E., Humphreys, E.D., Johnston, A.D., 1990. Anatexis and metamorphism in tectonically thickened continental crust exemplified by the Sevier hinterland, western North America. *Earth and Planetary Science Letters* 97, 290–315.
- Peslier, A.H., Reisberg, L., Ludden, J., Francis, D., 2000a. Os isotopic systematics in mantle xenoliths; age constraints on the Canadian Cordillera lithosphere. *Chemical Geology* 166, 85–101.
- Peslier, A.H., Reisberg, L., Ludden, J., Francis, D., 2000b. Re–Os constraints on harzburgite and lherzolite formation in the lithospheric mantle: a study of northern Canadian Cordillera xenoliths. *Geochimica et Cosmochimica Acta* 64, 3061–3071.
- Poirier, J.-P., 2000. *Introduction to the Physics of the Earth's Interior*. Cambridge University Press.
- Pollack, H.N., Chapman, D.S., 1977. On the regional variation of heat flow, geotherms, and lithospheric thickness. *Tectonophysics* 38, 279–296.
- Pouchou, J.L., Pichoir, F., 1985. PAP $\varphi(\rho Z)$ procedure for improved quantitative microanalysis. *Microbeam Analysis*, pp. 104–106.
- Raudsepp, M., Pani, E., Dipple, G.M., 1999. Measuring mineral abundance in skarn: I. The Rietveld method using X-ray powder diffraction data. *Canadian Mineralogist* 37, 1–15.
- Rietveld, H.M., 1967. Line profiles of neutron powder-diffraction peaks for structure refinement. *Acta Crystallographica* 22, 151–152.
- Robinson, J.A.C., Wood, B.J., 1998. The depth of the spinel to garnet transition at the peridotite solidus. *Earth and Planetary Science Letters* 164, 277–284.
- Ross, J.V., 1983. The nature and rheology of the Cordilleran upper mantle of British Columbia: inferences from peridotite xenoliths. *Tectonophysics* 100, 321–357.
- Shaw, C.S.J., Thibault, Y., Edgar, A.D., Lloyd, F.E., 1998. Mechanisms of orthopyroxene dissolution in silica-undersaturated melts at 1 atmosphere and implications for the origin of silica-rich glass in mantle xenoliths. *Contributions to Mineralogy and Petrology* 132, 354–370.
- Shi, L., Francis, D., Ludden, J., Frederiksen, A., Bostock, M., 1998. Xenolith evidence for lithospheric melting above anomalously hot mantle under the northern Canadian Cordillera. *Contributions to Mineralogy and Petrology* 131, 39–53.
- Snyder, D.B., Clowes, R.M., Cook, F.A., Erdmer, P., Evenchick, C.A., van der Velden, A.J., Hall, K.W., 2002. Proterozoic prism arrests suspect terranes: insights into the ancient Cordilleran margin from seismic reflection data. *GSA Today* 12 (10), 4–10.
- Turcotte, D.L., Schubert, G. (Eds.), 2002. *Geodynamics*, Second ed. Cambridge University Press.
- Wells, P.R.A., 1977. Pyroxene thermometry in simple and complex systems. *Contributions to Mineralogy and Petrology* 62, 129–139.
- Whitney, J.A., 1988. The origin of granite; the role and source of water in the evolution of granitic magmas. *Geological Society of America Bulletin* 100 (12), 1886–1897.
- Wood, B.J., Banno, S., 1973. Garnet–orthopyroxene and orthopyroxene–clinopyroxene relationships in simple and complex systems. *Contributions to Mineralogy and Petrology* 42, 109–124.